Title

Substituent Effects on the Coordination Chemistry of Metal-Binding Pharmacophores

Journal

Inorganic Chemistry, 56(19)

ISSN

0020-1669

Authors

Craig, Whitney R
Baker, Tessa W
Marts, Amy R
et al.

Publication Date

2017-10-02

DOI

10.1021/acs.inorgchem.7b01661

Peer reviewed

HHS Public Access

Author manuscript

Inorg Chem. Author manuscript; available in PMC 2019 April 30.

Published in final edited form as:

Inorg Chem. 2017 October 02; 56(19): 11721–11728. doi:10.1021/acs.inorgchem.7b01661.

Substituent Effects on the Coordination Chemistry of Metal-Binding Pharmacophores

Whitney R. Craig[†], **Tessa W. Baker**[†], **Amy R. Marts**[†], **Daniel T. DeGenova**[†], **David P. Martin**[‡], **Garrett C. Reed**[†], **Robert M. McCarrick**[†], **Michael W. Crowder**[†], **Seth M. Cohen**[‡], and **David L. Tierney**[†]

[†]Department of Chemistry and Biochemistry, Miami University, Oxford, Ohio 45056

[‡]Department of Chemistry and Biochemistry, University of California, San Diego, La Jolla, California 92093

Abstract

The combination of XAS, UV-vis, NMR and EPR was used to examine the binding of a series of α-hydroxythiones to CoCA. All three appear to bind preferentially in their neutral, protonated forms. Two of the three clearly bind in a monodentate fashion, through the thione sulfur alone. Thiomaltol (TM) appears to show some orientational preference, based on the NMR, while it appears thiopyromeconic acid (TPMA) retains rotational freedom. In contrast, allothiomaltol (ATM), after initially binding in its neutral form, presumably through the thione sulfur, forms a final complex that is five-coordinate complex via bidentate coordination of ATM. Based on optical titrations, we speculate that this may be due to the lower initial pK_a of ATM (8.3) relative to TM (9.0) and TPMA (9.5). Binding through the thione is shown to reduce the hydroxyl pK_a by ~ 0.7 pH units on metal binding, bringing only ATM's pK_a close to the pH of the experiment, facilitating deprotonation and subsequent coordination of the hydroxyl. The data predict the presence of a solvent-exchangeable proton on TM and TPMA, and Q-band 2-pulse ESEEM experiments on CoCA+TM suggest the proton is present. ESE-detected EPR also showed a surprising frequency dependence, giving only a subset of the expected resonances at X-band.

Graphical Abstract

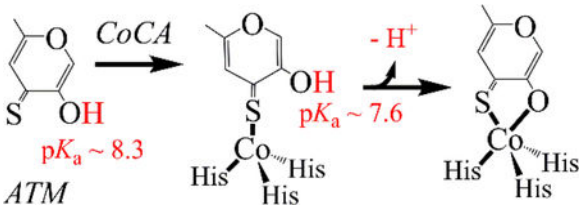

Corresponding Author: David L. Tierney tiernedl@miamioh.edu 513-529-8234.

Supporting Information. Detailed EXAFS fitting results are presented (Figures S1- S4, Tables S1- S4), along with pH-dependent MBP optical spectra (Figure S5), expanded views of fits to the optiocal titrations (Figure S6), an expanded view of the CoCA+TPMA NMR spectrum (Figure S7) and ESEEM time traces (Figure S8).

INTRODUCTION

Metalloproteins comprise up to fifty percent of all proteins, with Zn(II) containing enzymes the most widespread in diversity of function.(*1–3*) Consequently, Zn(II)-containing enzymes are attractive therapeutic targets for infirmities from bacterial infections to arthritis. Enzyme inhibitors that have found success are generally based on a metal-binding pharmacophore (MBP) as a scaffold, and the incorporation of pendant groups to facilitate secondary interactions.(4) Until recently, MBP design has mainly focused on thiols, carboxylic acids and hydroxamic acids.(4) Structure-aided rational design, as applied to metalloproteins, has been utilized to identify next generation MBPs for a number of enzymes,(5) and the three α-hydroxythiones of Figure 1 have proven potent inhibitors of MMPs.(6)

In a preceding study, we examined the binding of 5-hydroxy-2-methyl-4H-pyran-4-thione (allothiomaltol, ATM), 3-hydroxy-2-methyl-4H-pyran-4-thione (thiomaltol, TM), and 3-hydroxy-4H-pyran-4-thione (thiopyromeconic acid, TPMA) to Zn^{2+}-containing carbonic anhydrase.(7) The MBPs, as shown in Figure 1, differ in the presence or position of a methyl group. Using a combination of crystallography, X-ray absorption spectroscopy (XAS), and density functional theory (DFT) calculations, we showed that two of the three (TM and TPMA) bind exclusively as monodentate ligands through the thione sulfur. Steric clash limited the positioning of bound TM, allowing only two orientations that were roughly equally occupied, while the third MBP (ATM), binds in the expected bidentate fashion. In an effort to understand what led to mono- vs. bidentate coordination, we examine the same MBPs, this time with the Co(II)-containing enzyme (CoCA). Using XAS, optical, NMR and EPR spectroscopy, we show that the enzyme preferentially binds the neutral form of the MBP through the thione, and that the resulting shift in the hydroxyl pK_a is the determining factor for mono- vs. bidentate coordination.

EXPERIMENTAL

Materials

Commercially available, lyophilized CA-II from bovine erythrocytes (Sigma) was used for all of the studies presented here, as purchased; all reagents were used, as purchased, without further purification. All buffer solutions were made with 18.1 MΩ water from a Barnstead NANOpure system. Metal-binding pharmacophores (MBPs) were prepared according to published procedures.(7) All MBP complexes for spectroscopy were prepared with 2 molar equivalents of the MBP, at the stated concentrations.

Preparation of Co(II)-substituted CA-II

CA-II was dissolved at ~ 10 mM in Chelex-treated (Sigma Chelex® 100 sodium form) 50 mM phosphate buffer, pH 7.5 (referred to as “phosphate buffer” from here out). The concentrated protein was dialyzed for 48 h total against 4 × 2 L of phosphate buffer containing a 10-fold excess of 2,6-pyridinedicarboxylic acid. The resulting apo-CA-II contained less than 0.05 molar equivalents of Zn(II), from ICP-MS. Five molar eq of Co(II) (10 mM $CoCl_2 \cdot 6H_2O$; 99.999 %, Strem Chemicals) were added, and the mixture was incubated at 4 °C for 30 min. To remove excess metal, the protein mixture was treated with

30 % (v/v) of Chelex-contacting phosphate buffer (pH 7.5) for 15 min. Co(II)-substituted CA (CoCA) was then isolated from the Chelex using a small volume gravity flow column.

X-Ray Absorption Spectroscopy

Samples for EXAFS (~ 1.5 mM) were prepared with 20% (v/v) glycerol as a glassing agent. Samples were loaded into Lucite cuvettes with 6 μm polypropylene windows, and frozen in liquid nitrogen. Data were collected at the National Synchrotron Light Source (NSLS), beamline X3B, using a Si(111) double-crystal monochromator. Harmonic rejection was accomplished using a Ni focusing mirror. Fluorescence excitation spectra were measured with a 31-element solid-state Ge detector array; samples were held at approximately 15 K using a Displex cryostat. EXAFS data collection and reduction was performed according to published procedures (8) Duplicate data sets were collected for each sample, eight scans per sample. As the individual data sets gave similar results they were averaged; it is these average data that are presented here. Conversion from energy to *k*-space used E_0 = 7735 eV for the Co K-edge. EXAFS data were fitted using the nonlinear least-squares engine of IFEFFIT (distributed with SixPack, available free of charge from http://www-ssrl.slac.stanford.edu/~swebb/sixpack.html). Theoretical amplitude and phase functions were calculated with FEFF v. 800.(9)

UV-visible Spectroscopy

Optical spectra were obtained using a Perkin-Elmer Lambda 750 spectrophotometer. Quartz cuvettes (Perkin-Elmer; 1 cm path length) were used; the spectrometer was blanked against Chelex-filtered 50 mM, phosphate buffer, pH 7.5. MBP pK_a values were determined by monitoring the optical spectrum of a 78 μM solution as a function of pH, and fitting the resultant pH-dependent absorbance values to a modified form of the Henderson-Hasselbach equation. Binding assays were conducted by the addition 0.1–3.0 molar equivalents of selected the MBP.

NMR Spectroscopy

NMR samples were prepared using 50 mM phosphate, at pH (pD) 7.5, made with 99.9% D_2O (Cambridge Isotopes) and concentrated by centrifugation (Millipore Amicon® Ultra 15). Spectra were collected on ~1.5 mM samples with a Bruker ASX 200 NMR spectrometer (ν_H = 200.13 MHz) at approximately 290K. Water suppression was accomplished using a long, low-power pulse (100–150 ms, ~1 W) on the water signal, before moving the transmitter frequency to the region of interest for data collection.(10) Spectra were acquired using a 3 μs pulse at full power, and referenced to the residual water resonance at 4.7 ppm. Titrations were conducted by the addition of 0.5, 1, 2, and 3 molar equivalents of the selected MBP. Each spectrum consists of 4000 scans of 16k data points over a 75 kHz (375 ppm) window. All FIDs were apodized using a simple exponential that incorporated an additional 5 Hz line width.

EPR Spectroscopy

Low temperature X-band CW EPR spectra were collected using a Bruker EMX EPR spectrometer, equipped with an ER4116DM dual-mode cavity. Samples (~ 1.5 mM CoCA)

contained ~ 20 % (v/v) glycerol as a glassing agent. The spectra presented here were recorded at 9.62 GHz using the following parameters: 20 μW microwave power, 10 G magnetic field modulation (100 kHz); time constant/conversion time = 82 ms; receiver gain = 1×10^5, 16 scans.

X- and Q- band electron spin-echo (ESE) detected EPR, ESEEM and Mims pulsed ENDOR spectra were acquired on a Bruker Elexsys E680 spectrometer, operating at 9.76 or 34.0 GHz. The X-band ENDOR spectra used MW pulse lengths = 16 ns, τ = 180 ns, RF pulse length = 6 μs (100 W), repetition rate = 1250 Hz. Each spectrum consists of 1024 points (15 kHz point spacing), with each point the average of 35000 transients (700 scans at 50 averages per scan). The Q-band ESEEM measurements averaged four scans, using MW pulse lengths = 12 ns, repetition rate = 1000 Hz, and consisted of 512 points, using 4 ns spacing and 2-step phase cycling. Q-band Mims ENDOR employed MW pulse lengths = 12 ns, τ = 180 ns, RF pulse length = 8 μs (100 W), repetition rate = 1000 Hz. Each spectrum consists of 512 points (30 kHz point spacing), with each point the average of 20000 transients (800 scans at 25 averages per scan).

RESULTS

In previous work on this set of MBPs interacting with native Zn(II)-containing CA, we used a combination of X-ray diffraction and X-ray absorption spectroscopy (XAS) to show that all three MBPs bind to the active site metal ion through the thione sulfur atom, and only allothiomaltol binds in a bidentate fashion (see Figure 1).(7) This is in contrast to model studies, which showed bidentate coordination of all three MBPs to a metal-trispyrazolylborate scaffold, and was attributed to steric interactions with the 2-methyl group of thiomaltol. Our interests here were to examine this more closely, using the Co(II)-substituted enzyme. We begin with XAS of CoCA and its complexes with TM, TPMA and ATM, as the XAS provides the only direct comparison between the Zn(II) and Co(II) enzymes.

XAS

The XANES region of the spectra is shown in Figure 2A. The MBP complexes show a clear shift to lower energy (~ 0.5 eV), consistent with the incorporation of a soft donor in the metal ion's coordination sphere; the shift is greatest for the ATM complex. This is also reflected in the 1s⟋⟍3d transitions shown in Figure 2B, where the center of gravity of the transition shifts nearly 1 eV to lower energy. Integration of the 1s⟋⟍3d transitions shows a clear shift to lower intensity on addition of an MBP, from 20.3 for CoCA to 12.1–16.1 for the MBG complexes. There is a much greater loss of 1s⟋⟍3d intensity to higher energy in the MBP complexes relative to the resting enzyme, suggesting much of the change can be attributed to the loss of an available higher-energy bound-state MO.

The EXAFS data also support the binding modes indicated in Fig. 1. A comparison of the EXAFS FTs is presented in Figure 2C, and the best fit results are summarized in Table 1. Detailed fitting results are presented in Supporting Information, Figures S1–S4 and Tables S1–S4. The CoCA data are well fit with the expected model of 4 low-Z (N/O) donors, including 3 histidine ligands (Fig. S1 and Table S1). Addition of TM leads to a broadening

of the first shell along with the appearance of a shoulder to high-R on the first-shell peak (consistent with addition of a sulfur ligand), and substantial diminution of the outer shell scattering. The curve fitting results for the TM complex show a nearly 50 % reduction in fit residual on inclusion of a Co-S interaction in the first shell, although the overall coordination number is poorly determined between $(N/O)_3S$ and $(N/O)_4S$ (Fig. S2 and Table S2). Fits to the outer shell scattering were less satisfactory, most likely due to destructive interference from Co-TM multiple scattering. This is in contrast to the TPMA complex EXAFS, which shows the same first shell effects, but nearly identical outer shell scattering. The curve fits support sulfur coordination, with an accompanying 58 % reduction in fit residual, while the coordination number is again poorly determined between $(N/O)_3S$ and $(N/O)_4S$ (Fig. S3 and Table S3).

The ATM complex, which showed the smallest 1s⁄—3d transition (Table 1), also showed the most dramatically altered first shell peak, which was broadened to lower R, suggestive of a greater variation in metal-N/O bond lengths, and gained a shoulder to high-R. The high-R component is consistent with sulfur coordination, based on a near 50 % reduction in fit residual (compare fits S4–2 and S4–5), but attempts to include distinct Co-N and Co-O shells did not significantly improve the fits. However, the ATM complex presents the only data set that shows a clear minimum at 5-coordination (compare fits S4–1 and S4–2 to S4–3, and S4–4 to S4–5). Multiple scattering fits to these data were again unsatisfying, likely due to competing Co-ATM multiple-scattering interactions, which should be more significant in a bidentate MBP complex.

UV-visible Spectroscopy

Optical titrations were performed to examine MBP binding to CoCA. The conjugated thione leads to strong **π-π*** transitions in the visible, between 350 and 400 nm (Figure S5). All three MBP spectra are strongly pH dependent, allowing for determination of the hydroxyl pK_a for each molecule. For TM and ATM, bands for the protonated (low pH, red spectra in Fig. S5), and deprotonated (high pH, blue spectra) forms are well resolved, whereas they overlap for TPMA. TPMA shows lower energy transitions at 415 (OH) and 476 (O^-) nm that proved difficult to analyze. However, based on the spectra in Fig. S5, the hydroxyl pK_a values (± 0.3) rank from TPMA highest at ~ 9.5, to TM at ~ 9.0 and ATM lowest at ~ 8.3. We note that the uncertainty in the TM pK_a is larger than the other two, as the spectrum taken with pH ~ pK_a shows the weakest absorbance. All three pK_a values are above physiological pH, indicating the protonated forms should predominate for all, although a significant amount (~15 %) of the deprotonated form should be present for ATM.

After establishing the MBP pK_a values and the wavelengths characteristic to their protonation state, CoCA was titrated with each MBP in increasing increments up to 3 molar equivalents. Figure 3 shows the full titrations, which show that both protonated and deprotonated MBPs accumulate in the solution, and we believe as discussed below, that the MBP, free in solution, is being probed at these wavelengths. However, a cursory examination of the ligand-field bands (**insets** to Fig. 3), shows that the optical titrations are consistent with buildup of the species identified by XAS. That is, both TM and TPMA, as they accumulate in solution, begin to shift the overall spectrum upwards, but they do not affect

the general shape of the ligand field bands, particularly for TPMA. This suggests that binding of TM and TPMA must preserve the original 4-coordinate structure of resting CoCA. Meanwhile, addition of a single molar eq of ATM very quickly all but abolishes the ligand field bands (only the 515 nm band remains discernible), consistent with an increase in the coordination number of the Co(II) ion. (11)

To explore the equilibria involved, we examined the buildup of the various species. Plots of change in of absorbance (ΔA) vs. concentration of the MBP are shown in Figure 4. The simplest curve is seen for TM (Fig. 4A). The TM data are well fit with a simple, single-site binding model, across the span of the data. Fits to ΔA_{356} (protonated) and ΔA_{386} (deprotonated) give similar binding constants of 350 and 480 μM, respectively, compared to a K_i of 1.4 mM for TM with ZnCA.(7) In contrast, the full TPMA titration can be fit, within error, with straight lines (dashed lines in Fig. 4B). However, closer inspection of the early points in the titration, at less than 1 molar eq of MBP, shows the expected influence of metal binding, and the data can be fit at 341 nm (this band is present for both protonated and deprotonated TPMA, and would therefore be an overall binding constant, at 198 μM) and 476 nm (deprotonated, 320 μM). The fits to the early titration suggest potentially tighter binding of TPMA than TM.

Surprisingly, CoCA appears to show a preference for the protonated form of ATM. The fit lines in Fig. 4C are both simple single-site fits, but the fit to ΔA_{354} (protonated form) includes an x-offset to allow for a lag in its appearance. The lag of ~ 9 μM ATM means the protonated form does not appear in solution up to that concentration. Again, we examined the early points in the titration (< 1 eq MBP) (Figure S6A). Similar fits to the first four data points (shown as solid lines) indicate fairly tight binding of ATM, compared to the fits from part C that are superimposed as dashed lines. Comparison of the two red lines makes the lag phase discussed above more apparent, supporting the suggestion that CoCA shows a preference for the protonated form of ATM.

To better understand the effect of metal binding on the optical spectra, we endeavored to convert these data first to concentrations and then mole fractions. We first assumed that the high and low pH spectra for each MBP (Figure S5) are limiting. That is, they were assumed to be fully protonated or deprotonated, which provides the extinction coefficients in Table 2. As is apparent in Table 2, the bands overlap. As a crude approximation, to convert ΔA in Fig. 4A–C to concentrations, we simply used the difference of ε_{OH} and ε_{O^-}, which should overestimate the correction. The resulting concentrations were converted to mole fractions, which are plotted vs. the concentration of MBP (Figure 4D). For each MBP, the data at high concentration is consistent with the pK_a values above (see Fig. S6B), while those at low MBP concentration (below the enzyme concentration) are all clearly shifted to favor the deprotonated form. We take this as indication that the spectra being monitored arise from MBP free in solution, which in turn implies that the presence of the enzyme shifts the apparent mole fractions by preferentially binding the protonated form of the MBP. On this assumption, we then used the first addition (3.75 μM) to calculate effective pK_a values of 8.3 (TM), 8.4 (TPMA) and 7.6 (ATM), corresponding to shifts of −0.7. −1.1 and −0.7 pH units in the hydroxyl pK_a when the thione coordinates. In the case of TM and TPMA, the shift in pK_a is insufficient to lead to deprotonation of the hydroxyl (which fails to coordinate), while

the shift to 7.6 places the ATM hydroxyl in good position to subsequently deprotonate and coordinate.

NMR Spectroscopy

Proton NMR titrations are shown in Figure 5. The spectrum of resting CoCA is characterized by a pair of intense ^{2}H-exchangeable resonances at 62 and 52 ppm, corresponding to the NH protons of the three coordinated histidines, along with broad resonances at 40 and 93 ppm, and a number of sharp lines between 20 and −10 ppm from secondary interactions within the active site. At 0.5 eq of TM (Fig. 5A), the His resonance at 52 ppm nearly disappears and new resonances appear at 68, 79 and 102 ppm. At 1 eq, the line at 52 ppm is fully attenuated, and further additions do not lead to further changes, showing that a tight 1:1 complex is formed at the 1.5 mM concentrations used for NMR. The breadth of the lines is consistent with retention of four-coordination, while the dramatic change in chemical shift pattern suggests there is some orientational ordering of bound TM, consistent with the crystallography of the Zn enzyme.(7) By comparison, addition of 0.5 eq of TPMA leads to only a small upfield shift of the 52 ppm resonance that shifts to its final position at 1 eq, again showing that a tight 1:1 complex is formed. The lack of significant chemical shift perturbations on TPMA binding, suggests that bound TPMA does not suffer the steric constraints displayed by TM.

These results are in stark contrast to the addition of ATM to CoCA, which leads to the appearance of a number of new resonances and some rearrangement of the His resonances. Three of these can be attributed to the constitutive protons of ATM, although it is not possible to assign the spectra at present. The appearance of a number of resonances between 35 and −20 ppm are indicative of strong second sphere interactions in the active site, while the sharpness of the lines is clearly suggestive of five-coordination.(12)

EPR Spectroscopy

To probe the symmetry of the Co(II) coordination environment, CW EPR spectra were collected for CoCA with two molar equivalents of each MBP (Figure 6). The spectrum of resting CA is well known, with effective g-values of $g_{1,2,3}$ = [5.45, 4.35, 2.29] (top line in Figure 6A). The data show each MBG leads to an increase in the rhombicity of the Co(II) EPR, through sharpening of the low field (g_1) feature and broadening of the higher field components. That is, both g_2 (~ 2000 G) and g_3 (~ 3500 G) appear to decrease (shift to higher field). While, it is clear that all of the spectra are dominated by the $M_S = \pm {}^1/_2$ doublet within the zero-field split $S = {}^3/_2$ manifold of a high-spin Co(II) ion, the complex line shapes, particularly in the g_3 region (see Fig. 6A, **inset**), made quantitative interpretation of the data difficult. For example, all the low-field (g_1) resonances of the MBP complexes carry what appears to be a broader underlying signal. Similarly, the g_3 region shows a small Cu(II) impurity, unintentionally introduced with the MBP, whose signal overlaps a significant portion of this region.

The studies presented above suggest that TM and TPMA should retain a strongly-coupled, ^{2}H-exchangeable proton, if the MBP hydroxyl remains protonated. To seek verification, we turned to pulsed-EPR, ENDOR and ESEEM (Figure 7). The 2-pulse ESE-detected EPR

spectra (Fig. 7A) are overlaid with the CW spectra of Fig. 6. Interestingly, none of the X-band ESE-EPR spectra (bold lines in Fig. 7A) contain contributions from g_1, while it is clearly detected at Q-band (dashed lines in Fig. 7A). Within the limits of the very short ESE relaxation times of these high-spin Co(II) complexes ($\tau < 250$ ns), we did not see significant modulation of the ESE-spectrum, suggesting this is not an ESEEM effect. We believe this difference speaks to the origins of the various transitions in the CW spectrum.(13) Neither CA, nor any of the MBG complexes, showed sufficiently long electron relaxation at 4.5 K to attempt advanced EPR experiments (ENDOR and ESEEM), except the TM complex.

As we were most interested in determining the protonation state of the metal-bound MBP, we first turned to ENDOR spectroscopy, which probes metal-nucleus interactions directly. As the protons we were looking for are solvent-exchangeable and five bonds from the metal, it is reasonable to expect that the metal-proton hyperfine coupling should be detectable. However, the Mims ENDOR spectra obtained at X-band (Fig. 7B), at the field positions marked in Fig. 7A, showed only a broad envelope of proton couplings; we were unable to obtain suitably comparable spectra at the same field positions in D_2O, precluding further analysis. Experiments at Q-band gave similar results, with no detectable solvent-exchangeable proton ENDOR intensity with $A_H < 13$ MHz (Fig. 7B). The Q-band spectra show clear evidence that a relatively strongly-coupled, non-exchangeable proton is present, but it was not practical to pursue, as the spectra in Fig. 7 each required 8 or more hours of signal averaging. However, while the ENDOR failed to show evidence of an exchangeable proton, 2-pulse ESEEM of the TM complex very clearly showed evidence that the metal site is indeed interacting with a minimum of one deuteron. As shown in Fig. 7C, 2-pulse ESEEM at several fields give rise to a peak at the ^2H Larmor frequency, as well as a double-quantum peak. The H/D comparison was of high enough quality that the data could be ratioed, and the resulting FTs (bottom of Fig. 7C) follow what is apparent from the direct comparison above. While this could represent a matrix effect, as noted in the limited field-dependent dataset of Fig. 7C, the ^2H combination peaks are clearly offset from $2\nu_D$, suggesting the exchangeable proton experiences a non-negligible hyperfine interaction. All attempts to extend these data into 3-pulse ESEEM were unsuccessful, due to loss of signal over the course of the pulse sequence.

DISCUSSION

MBG Binding

Our previous work on these MBPs focused heavily on the interaction of TM with ZnCA.(7) In those studies, a combination of X-ray diffraction (solid-state structure) and XAS (frozen solution) were used to examine MBP binding, showing that each MBP in Fig. 1 binds preferentially through the neutral thione sulfur atom. This was surprising, given the presence of an ionizable hydroxyl on the adjacent carbon atom. The XAS studies presented here show that these binding modes are recapitulated in the Co(II)-substituted enzyme.

Crystal structures of TM bound to ZnCA showed preference for two specific binding orientations, rotationally related about the Zn-S bond.(7) Both orientations included a significant flattening of the TM plane, relative to the trigonal axis defined by the three coordinated His ligands, and DFT showed this leads to substantially weaker M-S bonding

than expected. However, the optical studies presented here (Figs. 3, 4, S5 and S6; Table 2) show that TM (pK_a = 9.0) coordinates almost exclusively as a neutral molecule, with a protonated hydroxyl that should be no better donor than the neutral thione, leading to the MBP's initial coordination via the sulfur. However, while binding of the thione to the metal lowers the hydroxyl pK_a by ~ 0.7 units, the shift is insufficient to favor deprotonation, and the neutral oxygen does not coordinate. Similar arguments can be made with regard to TPMA binding. The apparent shift in pK_a is larger on initial binding of the thione (ΔpK_a = 1.1), but it only lowers the effective pK_a to 8.4.

The orientational preference exhibited in the solid state by the ZnCA-TM complex is evident in substantially broadened ^{1}H NMR spectra (Fig. 5A). The tilting of the TM ring plane relative to the trigonal axis renders the three His ligands symmetry distinct, leading to three broad lines, and one would expect three resonances to come from a coordinated TM. The 2 eq spectrum shows the highest S/N and indicates at least 8 hyperfine shifted resonances. This is consistent with two mirror-related orientations for TM, which would lead to two magnetically inequivalent sets of three lines from TM, and up to 9 lines total. We note here that the EXAFS-determined Co-S distance is more consistent with a Co(II)-thiolate interaction, which would be consistent with tilting of the TM ring plane with respect to the Co-S-C. Resonance rearrangement in TM, from thione to thiolate sulfur, would eliminate rotational restrictions imposed by being part of the conjugated π-system. In contrast, TPMA appears to show no orientational preference, and this is reflected in its NMR spectra, which showed only a small perturbation of one of the His resonances, and a shorter Co-S distance of 2.25 Å from EXAFS, implying different electronic structure for the sulfur. The above predicts that both TM and TPMA bind preferentially in their neutral forms, but we were unable to see an ENDOR signature consistent with this expectation, largely due practical reasons. However, we see clear evidence for interaction of a solvent-exchangeable proton by H/D ESEEM at Q-band (Fig. 7C), and we are continuing work to identify it.

In contrast to TM and TPMA, allothiomaltol (ATM), with its pendant methyl group *trans* to the hydroxyl group, has an inherently lower p*K*a and metal binding by the thione is sufficient to shift the pKa in favor of deprotonation. This results in the originally expected bidentate binding mode, and a five-coordinate active site metal ion. This scenario best illustrated by the effect of ATM on CoCA's ligand field bands (Fig. 3), which all but disappear on addition of one eq of ATM, and its ^{1}H NMR spectrum, which shows a number of new resonances consistent with a change in metal-site geometry and line widths that are consistent with five-coordination (Fig. 5). ATM is the MBP that shows the clearest preference for binding the neutral form, with an obvious lag in the protonated form appearing in solution (Figs. 4C and S6A). This leads to an inversion of the apparent populations that is quickly returned to equilibrium once the enzyme is saturated (Fig. 4D). The importance of binding the neutral form of the MBP, we believe, is a consequence of the active site architecture. The generally hydrophobic second sphere of CA would disfavor approach of such a large charged species. However, once thione-coordinated, if the pK_a of the neighboring hydroxyl is sufficiently lowered, it can deprotonate and coordinate. It is tempting to suggest that binding of the neutral form provides a convenient source of a proton to facilitate dissociation of the resting state solvent, but that general mechanism would leave all three MBPs deprotonated, and we would therefore expect all three to be bidentate.

Consequently, we believe this is purely a thermodynamic effect, and affords the opportunity to consider new ways to tune the reactivity of a pharmacophore, once is has reached its target.

CW vs. Pulsed EPR

It is worth comment that the EPR responses of the resting enzyme and its three MBP complexes was dramatically dependent on the excitation frequency (X- vs. Q-band) and the method of detection (CW vs. ESE). The CW spectra all show systematic perturbations on MBP-binding, but they are surprisingly similar to each other. However, on switching to ESE detection at X-band, none of the g_1 transitions were observed (Fig. 7). They were present in equivalent ESE-detected spectra at Q-band, but the complexity of the ESE signal suggests the presence of multiple underlying signals. We have previously suggested that this is the result of smaller than expected zero-field splittings, unaccounted for mixing of the $M_S = {}^1/_2$ and ${}^3/_2$ doublets and potentially intensity-stealing allowing nominally forbidden transitions within the $M_S = {}^3/_2$ level to be observed. All of these mechanisms would only serve to facilitate relaxation of the ESE, and we were extremely limited in the experiments that were feasible, due to very fast electron relaxation. We are particularly interested in exploring the regions where the X- and Q-band ESE spectra differ, as this is where we are most likely to be able to identify whether the observation is the result of signals from different electron-spin doublets, or it is simply a relaxation effect.

SUMMARY

The combination of XAS, UV-vis, NMR and EPR was used to examine the binding of a series of α-hydroxythiones to CoCA. All three appear to bind preferentially in their neutral, protonated forms. Two of the three clearly bind in a monodentate fashion, through the thione sulfur alone. Thiomaltol (TM) appears to show some orientational preference, based on the NMR, while it appears thiopyromeconic acid (TPMA) retains rotational freedom. In contrast, allothiomaltol (ATM) forms a five-coordinate complex via bidentate coordination. Based on optical titrations, we speculate that this may be due to the lower initial pK_a of ATM (8.3) relative to TM (9.0) and TPMA (9.5). Binding through the thione is shown to reduce the hydroxyl pK_a by ~ 0.7 pH units on metal binding, bringing only the pK_a value of ATM close to the pH of the experiment, facilitating deprotonation and subsequent coordination of the hydroxyl. The data predict the presence of a solvent-exchangeable proton on TM and TPMA, and Q-band 2-pulse ESEEM experiments on CoCA+TM suggest the proton may be present. ESE-detected EPR also showed a surprising frequency dependence, giving only a subset of the expected resonances at X-band. ““

Supplementary Material

Refer to Web version on PubMed Central for supplementary material.

Acknowledgements

This work was supported by the National Science Foundation (CHE-1509285 to MWC and DLT, and CHE-1152755 to DLT) and the National Institutes of Health (R01 GM098435 to SMC and P30-EB-009998 to the

Center for Synchrotron Biosciences from the National Institute of Biomedical Imaging and Bioengineering, which supported beamline X3B at the National Synchrotron Light Source).

REFERENCES

1. Thomson AJ and Gray HB “Bio-inorganic Chemistry” Curr. Opin. Chem. Biol 1998, 2, 155–158. [PubMed: 9667942]
2. Vallee BL and Auld DS “Active-Site Zinc Ligands and Activated H_2O of Zinc Enzymes” Proc. Nat. Acad. Sci. USA 1990, 87, 220–224. [PubMed: 2104979]
3. Vallee BL and Auld DS “Zinc Coordination, Function, and Structure of Zinc Enzymes and Other Proteins” Biochemistry 1990, 29, 5647–5659. [PubMed: 2200508]
4. Jacobsen JA, Jourden J. L. Major, Miller MT and Cohen SM “To bind zinc or not to bind zinc: An examination of innovative approaches to improved metalloproteinase inhibition” Biochim. Biophys. Acta 2010, 1803, 72–94. [PubMed: 19712708]
5. Jacobsen JA, Fullagar JL, Miller MT and Cohen SM “Identifying Chelators for Metalloprotein Inhibitors Using a Fragment-Based Approach” J. Med. Chem 2011, 54, 591–602. [PubMed: 21189019]
6. Puerta DT, Lewis JA and Cohen SM “New Beginnings for Matrix Metalloproteinase Inhibitors: Identification of High-Affinity Zinc-Binding Groups” J. Am. Chem. Soc 2004, 126, 8388–8389. [PubMed: 15237990]
7. Martin DP, Blachly P, Marts AR, Woodruff TM, Oliveira C. d., Tierney DL and Cohen SM“Unconventional Coordination Modes by Metal Chelating Fragments in a Metalloprotein Active Site” J. Am. Chem. Soc 2014, 136, 5400–5406. [PubMed: 24635441]
8. Tierney DL and Schenk G “X-Ray Absorption Spectroscopy of Dinuclear Metallohydrolases” Biophys. J 2014, 107, 1263–1272. [PubMed: 25229134]
9. Ankudinov AL, Ravel B, Rehr JJ and Conradson SD “Real Space Multiple Scattering Calculation and Interpretaton of XANES” Phys. Rev. B 1998, 58, 7565–7576.
10. Riley EA, Petros AK, Smith KA, Gibney BR and Tierney DL “Frequency-Switching Inversion-Recovery for Severely Hyperfine Shifted NMR: Evidence of Asymmetric Electron Relaxation in High-Spin Co(II)” Inorg. Chem 2006, 45, 10016–10018. [PubMed: 17140197]
11. Garmer DR and Krauss M “Ab Initio Quantum Chemical Study of the Cobalt d-d Spectroscopy of Several Substituted Zinc Enzymes” J. Am. Chem. Soc 1993, 115, 10247–10257.
12. Bertini I, Luchinat C and Parigi G, Solution NMR of Paramagnetic Molecules. Elsevier: Amsterdam, 2001.
13. Baum RR, James CD and Tierney DL, “Paramagnetic Resonance of High-Spin Co(II) in Biologically-Relevant Environments: Models to Metalloproteins” In Biological Magnetic Resonance, Hanson G, Berliner L, Eds. Springer: New York, 2017; Vol. 33, pp 33–54.

Synopsis

Binding of a series of structurally related α-hydroxythiones to cobalt carbonic anhydrase is investigated using XAS, UV-vis, NMR, and EPR (CW and pulsed). The data show that all three bind initially in their neutral forms through the thione sulfur, and all three see a reduction of OH pK_a on binding. However, only one pK_a shifts low enough to favor deprotonation at physiological pH, forming a five-coordinate complex with CoCA; the other two remain four-coordinate.

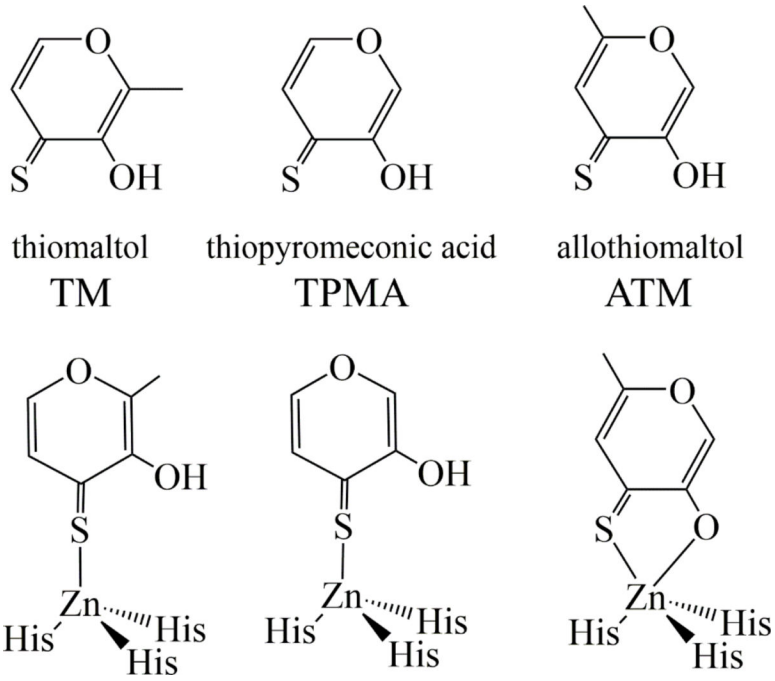

Figure 1.

Structures of metal binding pharmacophores (MBPs) under examination (*top*) and ZnCA binding modes observed previously (*bottom*).

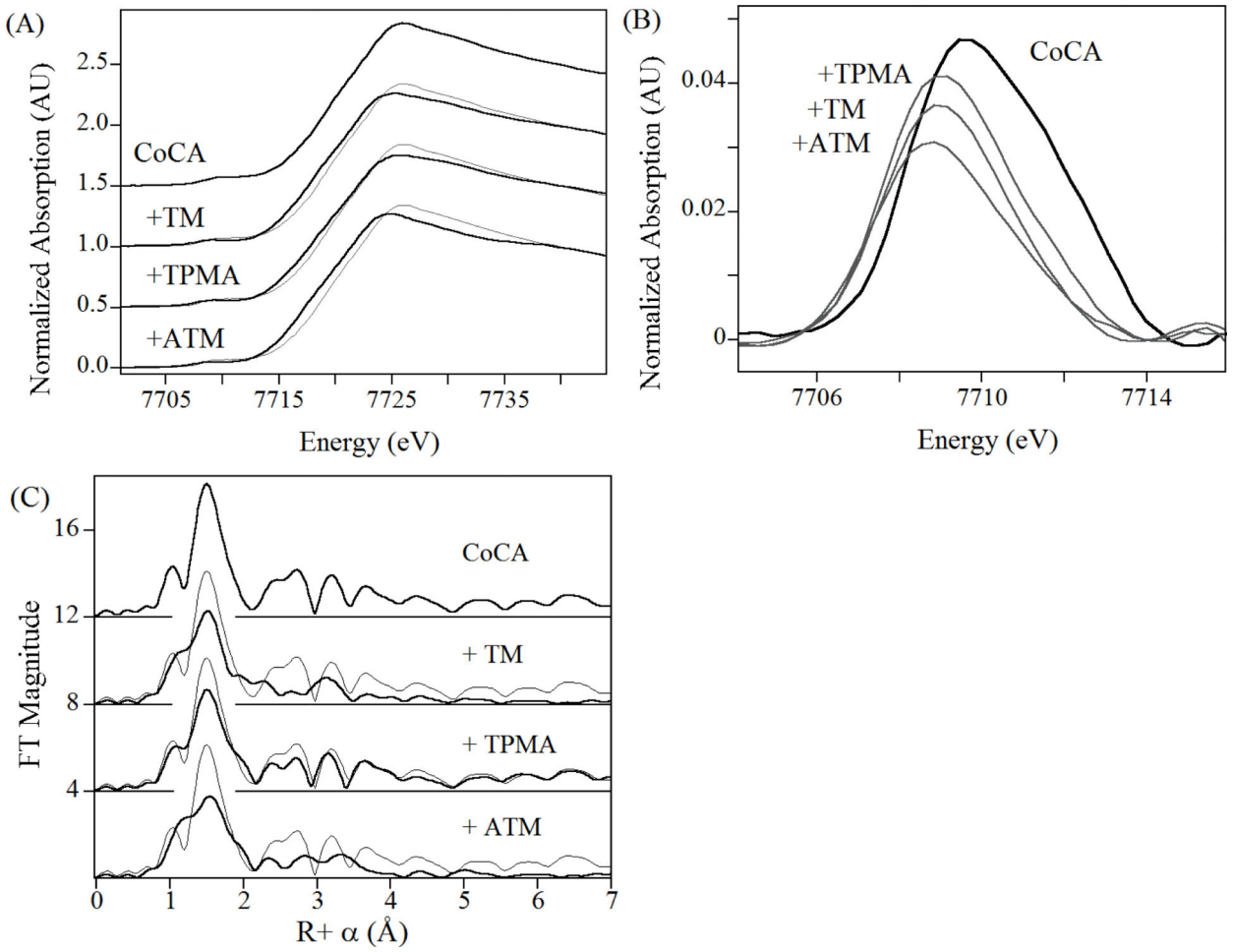

Figure 2.

X-ray Absorption spectroscopy of CoCA, and CoCA with added TM, TPMA and ATM. **(A)** XANES region. Each of the MBP-added spectra are overlaid with the CoCA spectrum (thin lines), for comparison. **(B)** 1s—3d transitions. CoCA is shown in black, while MBP-added data are shown in gray. **(C)** EXAFS Fourier transforms. Each of the MBP-added FTs are overlaid with the CoCA FT (thin lines) for comparison. Fitting results are summarized in Table 1.

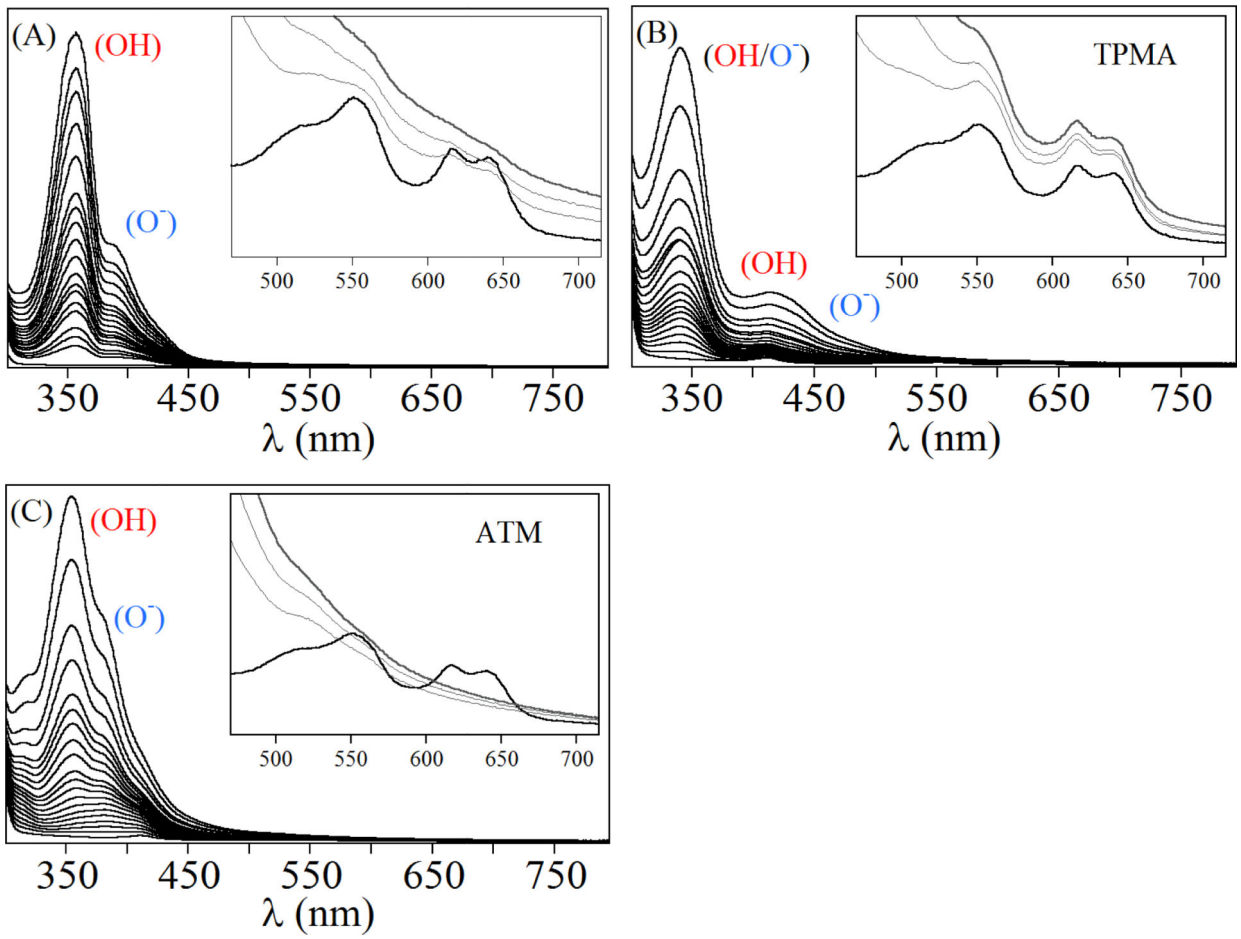

Figure 3.

Optical titration of 38 μM CoCA with increasing amounts of **(A)** thiomaltol, **(B)** thiopyromeconic acid and **(C)** allothiomaltol. Bands characteristic to the protonated (OH, red) and deprotonated (O^-, blue) state of the MBP are as indicated. **Insets**: Expansion of the ligand-field region of the spectra, with CoCA shown in black and successive additions of 1, 2 and 3 molar equivalents of the MBP in gray.

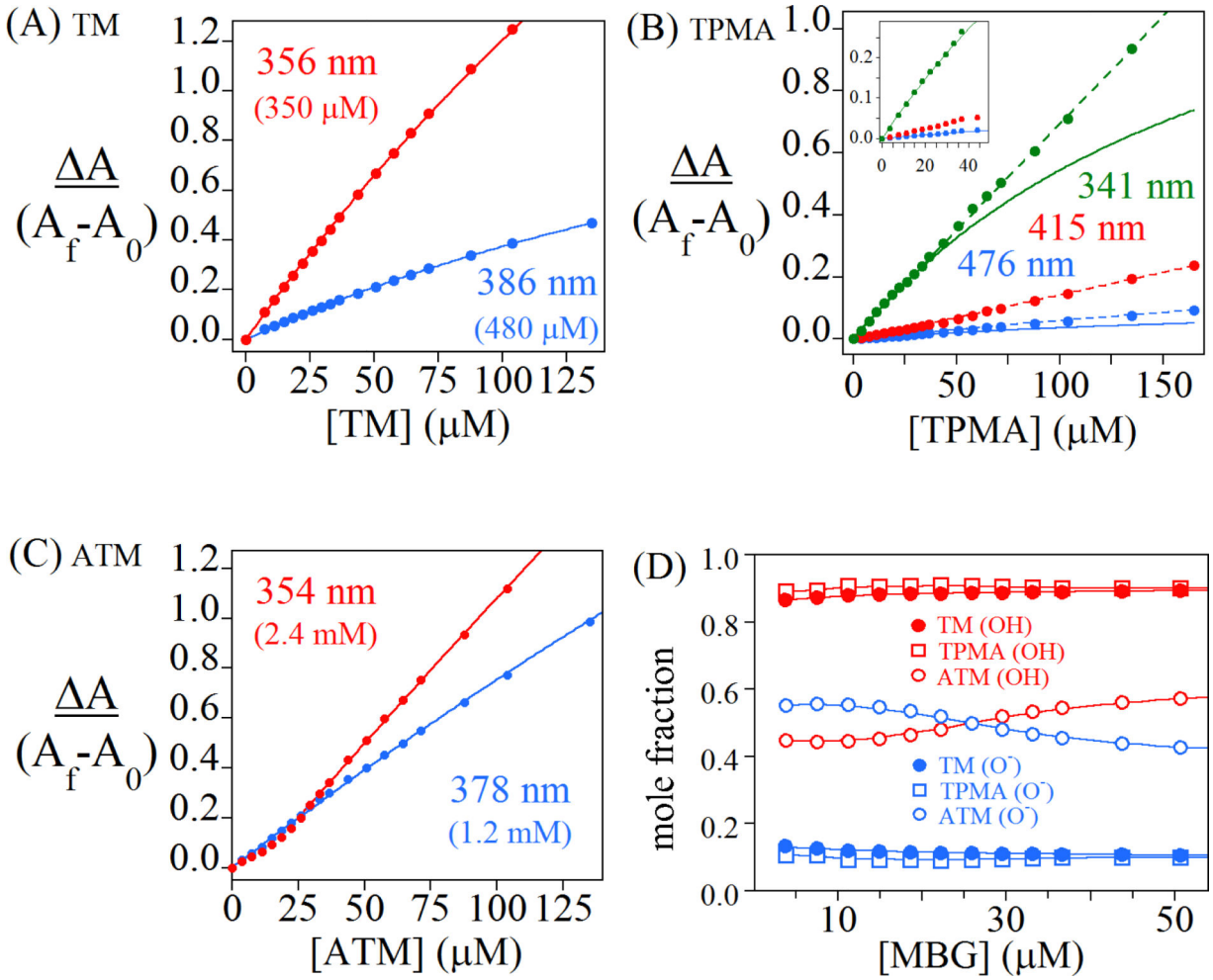

Figure 4.

Titrations of 38 μM CoCA with increasing amounts of **(A)** TM, **(B)** TPMA and **(C)** ATM. Red symbols indicate absorption bands associated with protonated MBP, blue symbols represent predominately deprotonated MBP bands and green symbols are used for bands that are overlapped for the two species. **(D)** Mole fractions of protonated and deprotonated MBP as a function of concentration added to 38 μM CoCA, as described in the text.

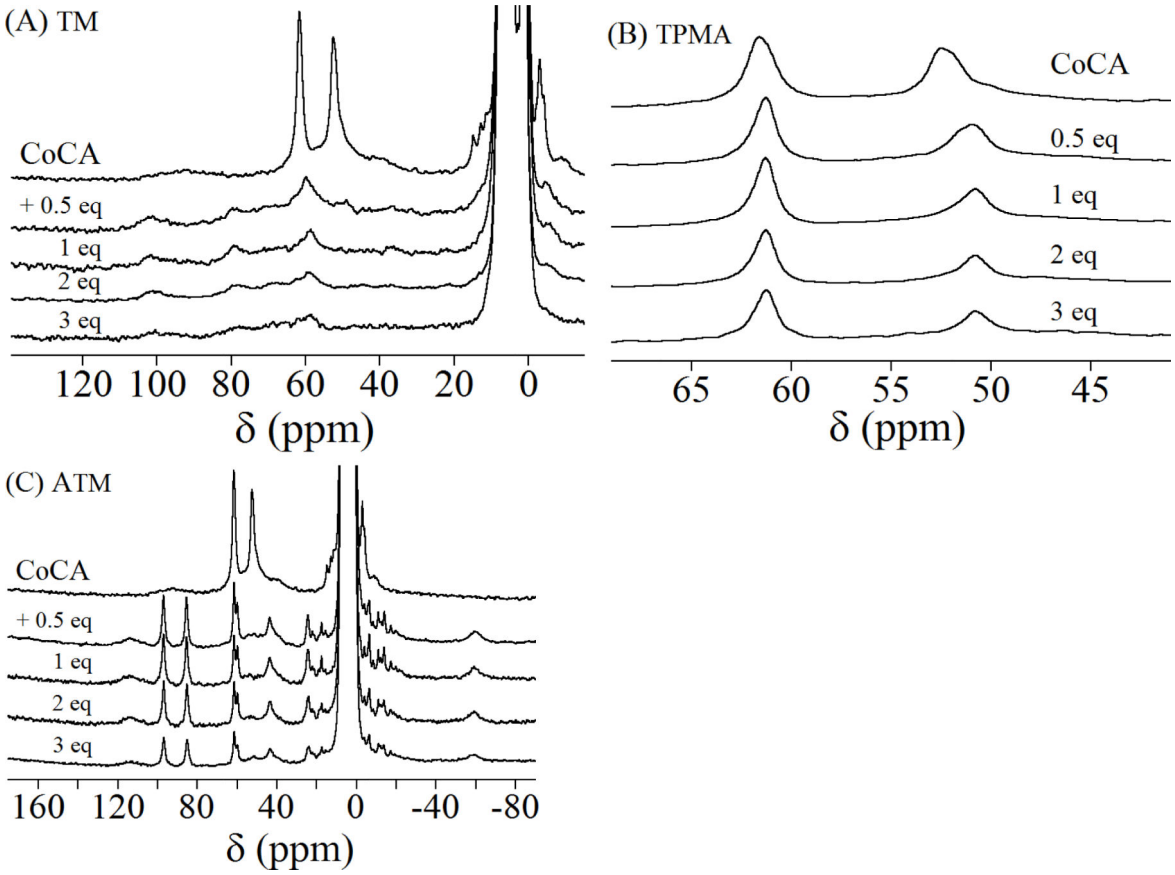

Figure 5.
200 MHz ^{1}H NMR of CoCA with increasing additions of MBP in 90 % H_2O.

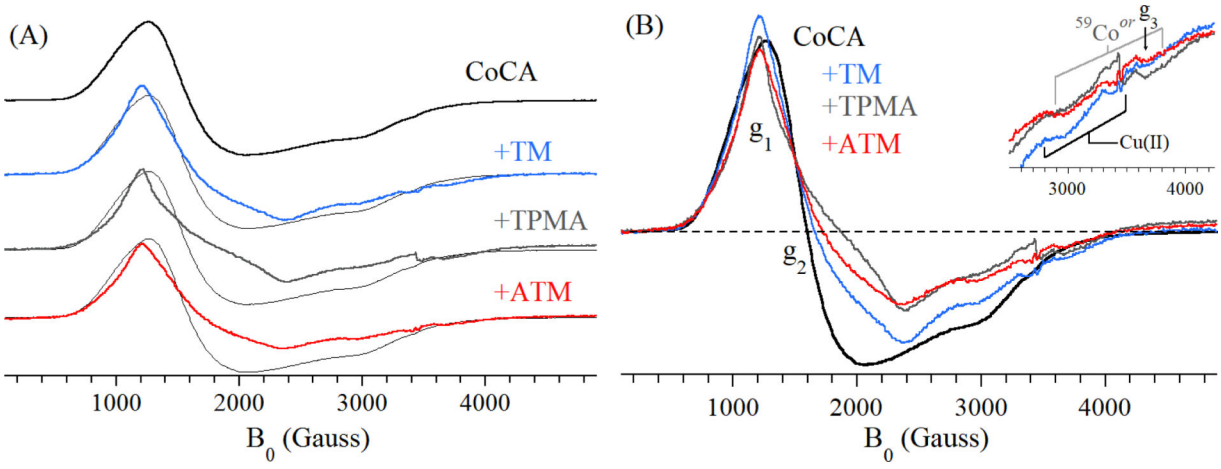

Figure 6.

X-band EPR spectra of CoCA, and CoCA in complex with 2 molar eq of the indicated MBP, both **(A)** offset vertically and **(B)** overlaid. **Inset to B**. Expansion of the g ~ 2 region, showing only the MBP complexes.

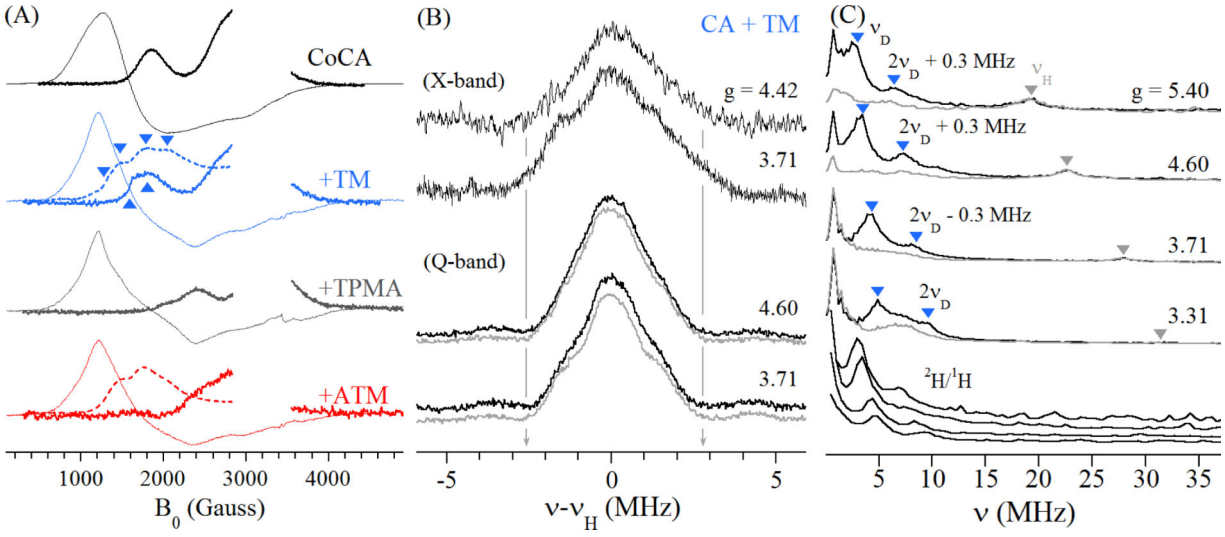

Figure 7.

Pulsed EPR of CoCA and its MBP complexes. **(A)** Comparison of CW (thin lines) and 2-pulse ESE-detected EPR at X- (thick lines) and Q-band (dotted lines). **(B)** X-band Mims pulsed ENDOR of CoCA + TM at X- (top) and Q-band (bottom) in H_2O (black) and D_2O (gray); fields, as indicated. The vertical arrows mark the Mims "**τ**-holes" at 2.8 MHz (**τ** = 180 ns at both frequencies). **(C)** Q-band 2-pulse ESEEM Fourier transforms for CoCA + TM in H_2O (gray) and D_2O (black). Inverted triangles mark the deuterium (blue) and proton (gray) Larmor frequencies; fields as indicated; bottom spectra are the D/H ratios described in the text and presented in the same order as above.

Table 1.

Best fits to CoCA+MBP EXAFS.

Sample	*Model*	*Fit*	1s⟋⟍3d area [a]
CoCA	4 N/O (2.02 Å)	S1–4	20.3
CoCA+TM	3 N/O (2.04 Å) + 1 S (2.29 Å)	S2–4	13.7
CoCA+TPMA	3 N/O (2.04 Å) + 1 S (2.25 Å)	S3–4	16.1
CoCA+ATM	4 N/O (2.09 Å) + 1 S (2.28 Å)	S4–5	12.1

[a] Areas in units 10^{-2} eV.

Table 2.

Optical parameters and binding constants from UV-vis titrations.

		(OH)			(O⁻)			
MBP	**pK_a**	**λ**	**ε**	**K_d** [a]	**λ**	**ε**	**K_d**	**K_i** [a,b]
TM	9.0	356	7700	0.35	386	12260	0.48	1.4
TPMA	9.5	415	990	0.20 [c]	476	780	0.32	1.1
ATM	8.3	354	14100	0.16	378	11850	0.16	0.65

[a] All values in mM.

[b] From Martin, et al [7].

[c] From fit to 341 nm data (ε = 9440 M^{-1} cm^{-1}), with contributions from both OH and O^- forms.

Table 3.

Apparent g-values from X-band EPR of CoCA and MBP complexes.

Sample	g_1	g_2	g_3
CoCA	5.45	4.35	2.29
+ TM	5.72	4.17	1.88 *or* 2.09
+ TPMA	5.72	3.73	1.88 *or* 2.09
+ ATM	5.68	4.01	1.88 *or* 2.09